RSC Advances

COMMUNICATION

View Article Online
View Journal | View Issue

Cite this: *RSC Adv.*, 2016, **6**, 35746

Received 28th January 2016
Accepted 24th March 2016

DOI: 10.1039/c6ra02530g

www.rsc.org/advances

Use of a novel layered titanoniobate as an anode material for long cycle life sodium ion batteries†

Keyu Xie,[a] Wenfei Wei,[a] Haoran Yu,[a] Manjiao Deng,[b] Shanming Ke,*[b] Xierong Zeng,[b] Zhihua Li,[c] Chao Shen,[a] Jian-gan Wang[a] and Bingqing Wei*[ad]

Sodium ion batteries have been attracting increasing attention as a replacement for lithium ion batteries in large-scale energy applications. However, it is proving difficult to find suitable sodium host materials with both a high capacity and excellent cycle stability. We prepared a layered titanoniobate (HTi_2NbO_7) *via* solid-state calcination followed by ion exchange for use in sodium ion batteries. The lamellar HTi_2NbO_7 had a specific capacity of about 90 mA h g^{-1} at 100 mA g^{-1}. The capacity was highly reversible over 2000 cycles. These results show that this lamellar titanoniobate material is a promising anode material for sodium ion batteries with a long cycle life.

Sodium ion batteries have been attracting much attention as a replacement for lithium ion batteries as a result of the low cost and high abundance of sodium resources.[1] When used in large-scale energy storage systems, where cost and sustainability are major concerns, the superiority of sodium ion batteries over their lithium ion counterparts becomes important.[2,3] However, it is difficult to find a suitable electrode material for sodium ion batteries as a result of the large ionic radius of sodium (70% larger than that of lithium).

A number of transition metal oxides show promise for electrochemical energy storage.[4] Titanium- and niobium-based oxides have been widely investigated as anode materials for lithium ion batteries as a result of the beneficial redox potentials of Nb^{5+}/Nb^{4+}, Ti^{4+}/Ti^{3+} and Nb^{4+}/Nb^{3+}.[5–7] A mixed titanium–niobium oxide ($TiNb_2O_7$) used as a novel anode for lithium ion batteries had a high theoretical capacity of up to 387.6 mA h g^{-1}.[8] This mixed titanium–niobium oxide has all the above-mentioned redox couples (Nb^{5+}/Nb^{4+}, Ti^{4+}/Ti^{3+} and Nb^{4+}/Nb^{3+}). As a result, a high specific capacity is expected because five lithium ions can theoretically be inserted into one formula unit of $TiNb_2O_7$. Other titanium–niobium oxide based materials, such as $Ti_2Nb_2O_9$,[9] $TiNb_2O_7$,[10,11] $TiNb_6O_{17}$ (ref. 12) and $Ti_2Nb_{10}O_{29}$,[13] have also been studied as electrode materials for lithium ion batteries and have shown excellent performance. Surprisingly, the family of titanium–niobium oxide based electrode materials also shows excellent insertion/extraction of lithium. $Ti_2Nb_{10}O_{29}$ has a reversible specific capacity of 238 mA h g^{-1} at 2C (1C = 396 mA g^{-1}) after 800 cycles.[13] However, as far as we know, there has been no report of the electrochemical properties of the mixed titanium–niobium oxide with multiple redox couples (Nb^{5+}/Nb^{4+}, Ti^{4+}/Ti^{3+} and Nb^{4+}/Nb^{3+}) for sodium intercalation.

In a similar manner, $Na_2Ti_3O_7$, which is also a member of the $A_xM_{2n}O_{4n+2}$ family of layered titanoniobates, should provide the possibility of lithium/sodium intercalation.[14] There have been few reports on sodium intercalation in these kinds of materials, which have both the easily reducible species Ti^{4+} and Nb^{5+} and a lamellar structure.[15] We report here the synthesis of the layered titanoniobate HTi_2NbO_7 *via* solid-state calcination followed by ion exchange and the first experimental results of the electrochemical properties of HTi_2NbO_7 as an anode material for sodium ion batteries. The preliminary results showed that HTi_2NbO_7 had a reversible specific capacity of about 90 mA h g^{-1} at 100 mA g^{-1} for sodium ion intercalation/de-intercalation after 2000 cycles.

Scheme 1 shows the manufacturing process for $HTi_2NbO_7 \cdot H_2O$. TiO_2, Nb_2O_5 and Cs_2CO_3 (a 10% molar excess) were first ground in a mortar for about 30 min and then heated at 1373 K for 12 h. A proton exchange reaction was then carried out by adding $CsTi_2NbO_7$ to an acidic solution (1 M) with magnetic stirring at 333 K for 24 h. The precipitate was filtered and washed three times with deionized water. HTi_2NbO_7 was obtained by heating the precipitate under vacuum at 423 K for 2 h.

[a]*State Key Laboratory of Solidification Processing and Center for Nano Energy Materials, Northwestern Polytechnical University, Xi'an, 710072, China. E-mail: weib@udel.edu*

[b]*Shenzhen Key Laboratory of Special Functional Materials, College of Materials Science and Engineering, Shenzhen University, Shenzhen 518060, PR China. E-mail: smke@szu.edu.cn*

[c]*School of Materials Science and Engineering, Central South University, Changsha, Hunan, 410083, China*

[d]*Department of Mechanical Engineering, University of Delaware, Newark, DE 19716, USA*

† Electronic supplementary information (ESI) available: Experimental details. See DOI: 10.1039/c6ra02530g

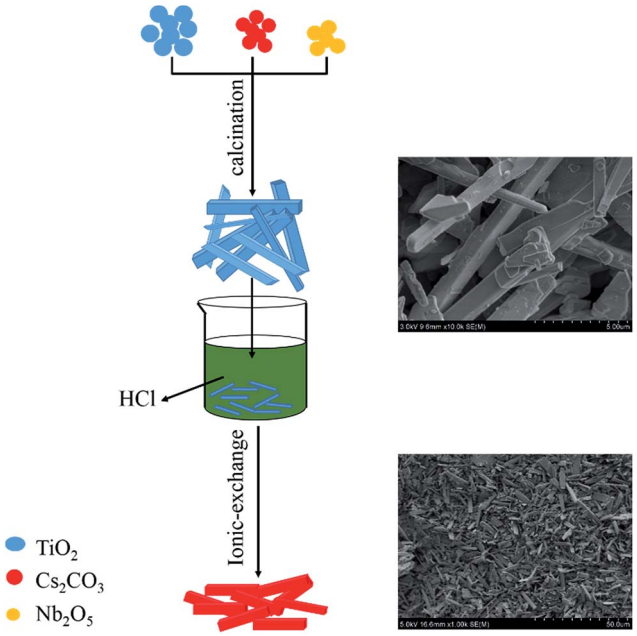

Scheme 1 Schematic diagram of the manufacture of $HTi_2NbO_7 \cdot H_2O$.

Fig. 1a and b shows the X-ray diffraction patterns of $CsTi_2NbO_7$ and HTi_2NbO_7, which match well with the orthorhombic crystallographic system;[16] all the diffraction peaks were in accordance with those of JCPDS Card no. 73-0680 and JCPDS Card no. 54-1154, respectively. These results show that there was no impurity in the products and the interlamellar spacing was reduced.[17] Fig. 1c shows the structure of HTi_2NbO_7. The H^+ structure is built up from layers containing zigzag strings with groups of three edge-shared octahedra. The strings are linked side by side *via* corner sharing to form $Ti_2NbO_7^-$ layers. The H^+ ions occupy distorted cubic sites between the layers. Two adjacent layers are related by a glide plane in both structures.[17]

The morphology of the cuboid arrangement is shown in Fig. 2a, the scanning electron microscopy (SEM) image, which

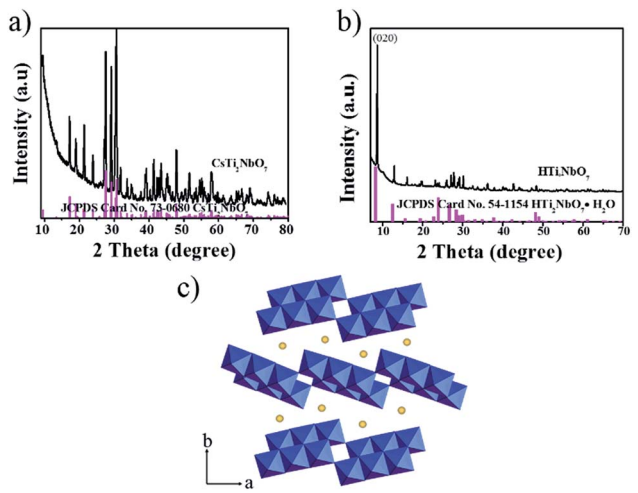

Fig. 1 XRD patterns of (a) $CsTi_2NbO_7$ and (b) HTi_2NbO_7. (c) Structure of layered HTi_2NbO_7.

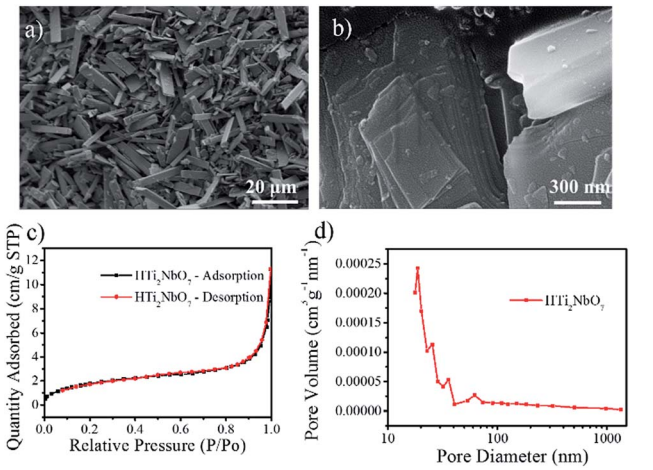

Fig. 2 SEM images of HTi_2NbO_7: (a) low-resolution SEM image of overall view; and (b) high-resolution SEM image of part of a cuboid. (c) Nitrogen adsorption–desorption isotherms of HTi_2NbO_7. (d) Pore size distribution curve for HTi_2NbO_7.

shows a uniform width distribution of ~2 μm. Fig. 2b clearly shows that the lamellar titanoniobate HTi_2NbO_7 has a layered structure. The nitrogen adsorption/desorption isotherm and pore size distribution plots show the characteristics of this mesoporous material (Fig. 2c and d). The material has a relatively low BET surface area of 6.7 $m^2\ g^{-1}$ and the pore size distribution is mainly from 2 to 3 nm. The mesoporous laminated structure could give a greater active area for Na^+.

XPS was used to investigate the surface composition and valence states of HTi_2NbO_7. Photoelectron peaks for C, O, Ti and Nb can been clearly seen in Fig. 3a. Fig. 3b confirmed the existence of the Ti^{4+} oxidation state from the Ti $2p_{1/2}$ and $2p_{3/2}$ peaks at 464.2 and 458.3 eV with a spin–orbit splitting of about 5.9 eV.[18] Fig. 3c shows the Nb 3d spectrum for HTi_2NbO_7, with two peaks at 206.8 and 209.5 eV. These two peaks represent the $3d_{5/2}$ and $3d_{3/2}$ components, respectively, with a spin–orbit splitting of 2.7 eV. The center of the Nb $3d_{3/2}$ peak corresponds to the Nb^{5+} oxidation state.[19]

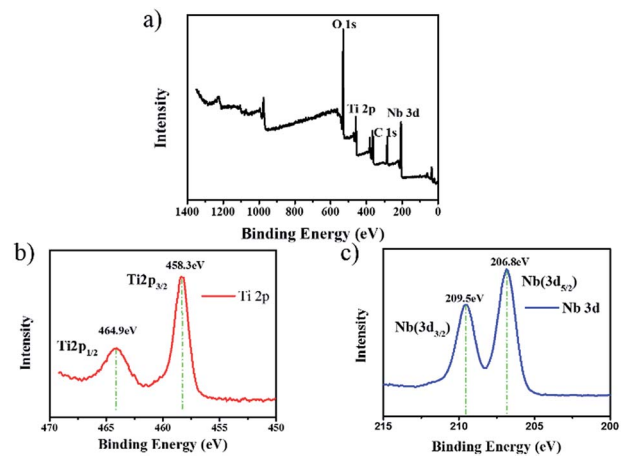

Fig. 3 (a) XPS survey spectra for the surfaces of the HTi_2NbO_7 sample. Typical spectra of (b) Ti 2p and (c) Nb 3d.

The electrochemical performance of the layered HTi_2NbO_7 anode were studied by galvanostatic charge–discharge measurements. Each cell was tested at potentials within the range 0.01–3 V. Fig. 4a shows the initial charge–discharge voltage profiles at 100 mA g^{-1}. The discharge curves show four different regions: two sloping regions at 1.5–1.25 and 0.98–0.86 V; a plateau at 0.45 V; and a further plateau region up to the discharge limit. The voltage decreased sharply to 1.5 V, mainly due to a solid solution reaction. The two sloping regions at 1.5–1.25 and 0.98–0.86 V and the plateau at 0.45 V are attributed to a two-phase reaction for Nb^{5+}/Nb^{4+}, Ti^{4+}/Ti^{3+} and Nb^{4+}/Nb^{3+}, respectively.[20] There is another long plateau from 0.16 to 0.01 V, which may correspond to the process in which H^+ ions are simultaneously replaced by Na^+ ions during the electrochemical intercalation.[15] During the first discharge, the specific capacity reaches 430 mA h g^{-1} with a reversible capacity of about 200 mA h g^{-1}. The irreversible capacity can be mainly attributed to the transformation of the structure resulting from the irreversible process of Na^+ replacing H^+ and the formation of the solid electrolyte interface (SEI).[15] From the tenth cycle, the capacity gradually become stable, showing that the structure tended to become steady after all the H^+ had been replaced by Na^+.

Cyclic voltammetry curves of the HTi_2NbO_7 anode at a scanning rate of 0.01 mV s^{-1} over the voltage range 0.01–3.0 V are shown in Fig. 4b. There are two small peaks around 1.5 and 0.98 V as a result of the valence variation of Nb^{5+}/Nb^{4+} and Ti^{4+}/Ti^{3+}; a sharp peak at 0.45 V could correspond to the Nb^{4+}/Nb^{3+} redox couple.[20] The last sharp sloping peak at 0.01 V may be due to the replacement of H^+ by Na^+. The CV curves are in agreement with the charge–discharge curves.

Long-term cycle stability is a challenge for practical sodium ion batteries as a result of the possible structural degradation of the host during cycling. Fig. 4c shows the superior cycling performance of the HTi_2NbO_7 electrode at 100 mA g^{-1}. Although a slow fading of capacity is seem in the initial few dozen cycles, there was no decline in capacity during the subsequent 2000 cycles. In addition, a reversible capacity of about 90 mA h g^{-1} remained unchanged during the subsequent 2000 cycles, indicating excellent cycle stability. With respect to the contribution of conductive carbon, the capacity of pure HTi_2NbO_7 is about 70 mA h g^{-1} (ESI, Fig. S1†). Notably, the layered structure of the HTi_2NbO_7 was almost unchanged after 2000 cycles, although it was covered with a thick SEI film (ESI, Fig. S2†). Correspondingly, the coulombic efficiency gradually increased during the initial cycles and remained at >99% in the following cycles. The performance of this HTi_2NbO_7 electrode is better than that of other materials reported for sodium ion batteries, such as Nb_2O_5 (about 30 mA h g^{-1} after 50 cycles at 50 mA g^{-1}),[21] $K_{0.8}Ti_{1.73}Li_{0.27}O_4$ (about 80 mA h g^{-1} at 100 mA g^{-1}),[22] $Na_{2/3}Co_{1/3}Ti_{2/3}O_2$ (50 mA h g^{-1} at 500 mA g^{-1}),[23] TiO_2 nanoparticles (93 mA h g^{-1} at 1700 mA g^{-1}),[24] $Na_2Ti_6O_{13}$ (about 100 mA h g^{-1} after 30 cycles at 5 mA g^{-1})[25] and $Cu_{0.5}TiOPO_4$ (70 mA h g^{-1} after 20 cycles at 42.2 mA g^{-1}).[26]

To further understand the electrochemical characteristics of HTi_2NbO_7, rate capability tests were performed at different current densities (Fig. 4d). A reversible capacity of 106 mA h g^{-1} was obtained at a low current density of 40 mA g^{-1}. When the current density increased to 100 and 200 mA g^{-1}, reversible specific capacities of 77 and 62 mA h g^{-1} were obtained respectively. Even though the current density increased to 1000 mA g^{-1}, a capacity of about 32 mA h g^{-1} was still maintained. When the current density reversed back to 40 mA g^{-1}, the capacity of the HTi_2NbO_7 still remained at about 85 mA h g^{-1}. Taking into account the contribution of conductive carbon, the capacity of pure HTi_2NbO_7 is reduced by a certain ratio. These results indicate that HTi_2NbO_7 has a good rate performance.

EIS was also carried out to obtain insights into the electrochemical behavior of HTi_2NbO_7. These data were recorded before cycling and after 100 cycles (Fig. 5). As Fig. 5a shows, the Nyquist plots consist of one semicircle at high frequencies and a straight line at low frequencies. Fig. 5b shows that the Nyquist plots consist of two anomalous semicircles at high frequencies after 100 cycles at 100 mA h g^{-1}. The equivalent circuit was used to determine the resistance of the cells after 100 cycles in detail (Fig. 5c). Table 1 shows the fitted EIS values of the equivalent circuit elements. The intercept at the real axis at high frequency gives the electrolyte resistance (R_s) for the battery.[27] The semicircle is usually attributed to the SEI film (R_{sei} and C_{sei}) and the charge transfer process through the electrode surface (R_{ct} and CPE(C_{dl})), respectively.[28] The straight line in the low frequency domain is the Warburg impedance (W), which is attributed to the diffusion of Na ions in the electrode.[29] There was no SEI film before cycling; after 100 cycles the radius of the semicircle at medium frequencies was smaller than that of the battery before cycling. The decrease in R_{ct} is attributed to the formation of a SEI film on the cycled electrode, which enhances the reaction kinetics, as reported previously.[30,31] The Warburg impedance of the battery after 100 cycles was much lower than that of the battery before cycling, which indicates that the polarization of the HTi_2NbO_7 anode decreased dramatically favors capacity retention during cycling.[32]

We have successfully fabricated a layered HTi_2NbO_7 structure *via* a solid-state reaction followed by ion exchange and used it as an anode material in sodium ion batteries. Electrochemical

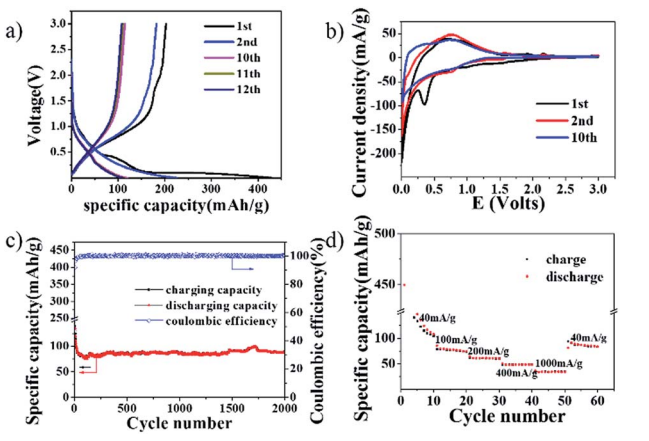

Fig. 4 (a) Galvanostatic discharge–charge profiles of HTi_2NbO_7 at 100 mA g^{-1}. (b) Cyclic voltammetry of HTi_2NbO_7 at a scan rate of 0.01 mV s^{-1}. (c) Cycle performance of HTi_2NbO_7 at 100 mA g^{-1}. (d) Rate performance for the HTi_2NbO_7 electrode.

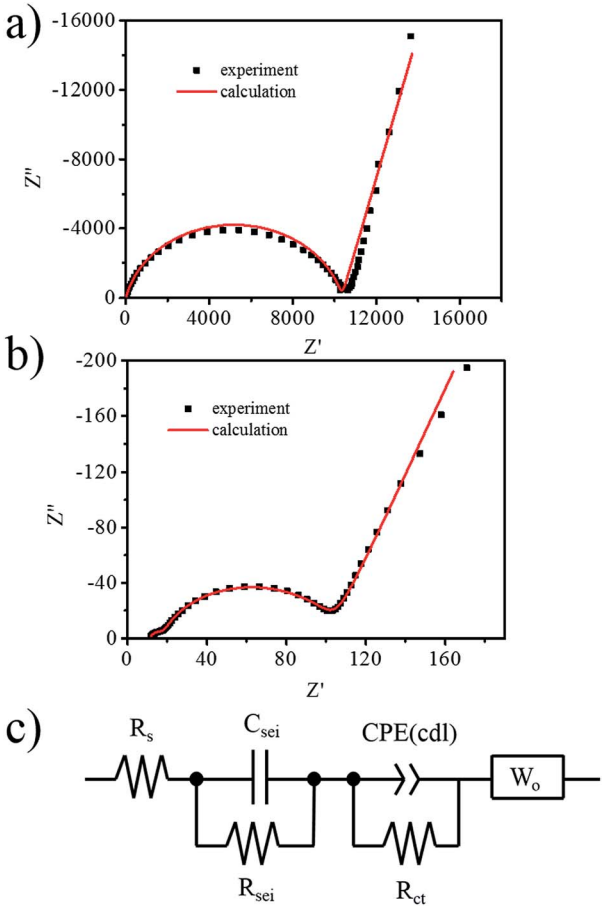

Fig. 5 Impedance plots of HTi_2NbO_7 for (a) before cycling and (b) after 100 cycles at 100 mA h g^{-1}. (c) Equivalent circuit for simulating the EIS data about the battery after 100 cycles.

Table 1 Fitted values for the HTi_2NbO_7 electrode after 110 cycles

Parameter	Value
R_s (Ω)	11.18
C_{sei}	1.3091×10^{-6}
R_{sei} (Ω)	5.364
CPE-T(C_{dl})	1.8005×10^{-5}
CPE-P(C_{dl})	0.89822
R_{ct}	77.67
W_o-R	23.53
W_o-T	0.017247
W_o-P	0.40037

tests indicated that this layered material can give a reversible capacity of about 90 mA h g^{-1} with no capacity fading after 2000 cycles in the voltage range 0.01–3.0 V. This is an exciting option for the synthesis and design of new materials with layered structures as high-performance anodes for sodium ion batteries. The material displayed excellent cycle performance and we believe that these results represent a significant step forward in the development of long-life sodium ion batteries for large-scale applications in novel energy storage devices.

Acknowledgements

The authors appreciate financial support from the National Natural Science Foundation of China (No. 51302219, 51472204, 51402236 and 51302172), the Shenzhen Key Laboratory of Special Functional Materials (T201504), the Natural Science Foundation of Shannxi Province (No. 2015JM2045), the Specialized Research Fund for the Doctoral Program of Higher Education of China (No. 20136102120024), the Research Fund of the State Key Laboratory of Solidification Processing (NWPU), China (Grant No. 06-QP-2014) and the Fundamental Research Funds for the Central Universities (No. 3102014JCQ01019).

Notes and references

1 V. Palomares, P. Serras, I. Villaluenga, K. B. Hueso, J. Carretero-González and T. Rojo, *Energy Environ. Sci.*, 2012, **5**, 5884–5901.
2 S.-W. Kim, D.-H. Seo, X. Ma, G. Ceder and K. Kang, *Adv. Energy Mater.*, 2012, **2**, 710–721.
3 M. D. Slater, D. Kim, E. Lee and C. S. Johnson, *Adv. Funct. Mater.*, 2013, **23**, 947–958.
4 J. Zhang and A. Yu, *Sci. Bull.*, 2015, **60**, 823–838.
5 M. A. Reddy and U. V. Varadaraju, *Chem. Mater.*, 2008, **20**, 4557–4559.
6 S.-H. Kang, D. P. Abraham, W.-S. Yoon, K.-W. Nam and X.-Q. Yang, *Electrochim. Acta*, 2008, **54**, 684–689.
7 J.-T. Han, D.-Q. Liu, S.-H. Song, Y. Kim and J. B. Goodenough, *Chem. Mater.*, 2009, **21**, 4753–4755.
8 J.-T. Han, Y.-H. Huang and J. B. Goodenough, *Chem. Mater.*, 2011, **23**, 2027–2029.
9 J.-F. Colin, V. Pralong, M. Hervieu, V. Caignaert and B. Raveau, *Chem. Mater.*, 2008, **20**, 1534–1540.
10 C. Jo, Y. Kim, J. Hwang, J. Shim, J. Chun and J. Lee, *Chem. Mater.*, 2014, **26**, 3508–3514.
11 B. Guo, X. Yu, X.-G. Sun, M. Chi, Z.-A. Qiao, J. Liu, Y.-S. Hu, X.-Q. Yang, J. B. Goodenough and S. Dai, *Energy Environ. Sci.*, 2014, **7**, 2220–2226.
12 C. Lin, G. Wang, S. Lin, J. Li and L. Lu, *Chem. Commun.*, 2015, **51**, 8970–8973.
13 Q. Cheng, J. Liang, Y. Zhu, L. Si, C. Guo and Y. Qian, *J. Mater. Chem. A*, 2014, **2**, 17258–17262.
14 J.-F. Colin, V. Pralong, V. Caignaert, M. Hervieu and B. Raveau, *Inorg. Chem.*, 2006, **45**, 7217–7223.
15 J. F. Colin, V. Pralong, M. Hervieu, V. Caignaert and B. Raveau, *J. Mater. Chem.*, 2008, **18**, 3121.
16 M. Hervieu and B. Raveau, *J. Solid State Chem.*, 1980, **32**, 161–165.
17 M. Lal and A. T. Howe, *J. Mater. Chem.*, 1984, **51**, 355–363.
18 C. Ban, M. Xie, X. Sun, J. J. Travis, G. Wang, H. Sun, A. C. Dillon, J. Lian and S. M. George, *Nanotechnology*, 2013, **24**, 424002.
19 M. Z. Atashbar, H. T. Sun, B. Gongc, W. Wlodarski and R. Lamb, *Thin Solid Films*, 1998, **326**, 238–244.
20 V. Aravindan, J. Sundaramurthy, A. Jain, P. S. Kumar, W. C. Ling, S. Ramakrishna, M. P. Srinivasan and S. Madhavi, *ChemSusChem*, 2014, **7**, 1858–1863.

21 H. Kim, E. Lim, C. Jo, G. Yoon, J. Hwang, S. Jeong, J. Lee and K. Kang, *Nano Energy*, 2015, **16**, 62–70.
22 K. Y. Chen, W. X. Zhang, Y. Liu, H. P. Zhu, J. Duan, X. H. Xiang, L. H. Xue and Y. H. Huang, *Chem. Commun.*, 2015, **51**, 1608–1611.
23 H. Yu, Y. Ren, D. Xiao, S. Guo, Y. Zhu, Y. Qian, L. Gu and H. Zhou, *Angew. Chem., Int. Ed.*, 2014, **53**, 8963–8969.
24 Z. Hong, K. Zhou, Z. Huang and M. Wei, *Sci. Rep.*, 2015, **5**, 11960.
25 K. Shen and M. Wagemaker, *Inorg. Chem.*, 2014, **53**, 8250–8256.
26 P. Bleith, H. Kaiser, P. Novák and C. Villevieille, *Electrochim. Acta*, 2015, **176**, 18–21.
27 S. A. Needham, G. X. Wang, K. Konstantinov, Y. Tournayre, Z. Lao and H. K. Liu, *Electrochem. Solid-State Lett.*, 2006, **9**, A315.
28 S. S. Zhang, K. Xu and T. R. Jow, *Electrochim. Acta*, 2004, **49**, 1057–1061.
29 K. Tang, L. Fu, R. J. White, L. Yu, M.-M. Titirici, M. Antonietti and J. Maier, *Adv. Energy Mater.*, 2012, **2**, 873–877.
30 K. Y. Xie, Z. G. Lu, H. T. Huang, W. Lu, Y. Q. Lai, J. Li, L. M. Zhou and Y. X. Liu, *J. Mater. Chem.*, 2012, **22**, 5560–5567.
31 Y. Liu, C. H. Mi, L. H. Su and X. G. Zhang, *Electrochim. Acta*, 2008, **53**, 2507–2513.
32 N. V. Nghia, P.-W. Ou and I. M. Hung, *Ceram. Int.*, 2015, **41**, 10199–10207.